# Non-linear Breakdown in Hypersonic Boundary Layer Transition Induced by Freestream Disturbances

Jia Lei[1] and Xiaolin Zhong[2]

*Mechanical and Aerospace Engineering Department, UCLA, Los Angeles, CA, 90095*

Prediction of Laminar-turbulent transition in hypersonic boundary layer is a very challenging task. For decades, lots of experimental, theoretical and numerical efforts have been made to seek a reliable method to predict transition. The most success is gained based upon the semi-empirical $e^N$ method. However, it does not take the initial amplitude of disturbances into account and highly relies on the experimental correlation. Due to the rapidly growing large scale computation capability, direct numerical simulation (DNS) has become a promising tool in assisting us to unveil the mystery of hypersonic boundary layer transition. In this paper, a new approach is presented to simulate the hypersonic boundary layer flow over a cone from laminar to the nonlinear breakdown using disturbance induced from the freestream waves. The goal is to develop a robust numerical tool that using a built linear receptivity library as inflow forcing to simulate the hypersonic boundary later flow to the non-linear breakdown stage and study the effects of freestream disturbance levels to the location of transition.

## Nomenclature

$a$      =    non-dimensional wave speed
$e$      =    total energy per unit volume
$Fi$      =    inviscid flux vector
$Fv$      =    viscous flux vector
$F$      =    frequency
$M$      =    Mach number
$Pr$      =    Prandtl number
$P$      =    pressure
$R_n$      =    nose radius
$Re$      =    Reynolds number
$Re_n$      =    Reynolds number based on the nose radius
$s$      =    distance along the cone surface from the nose tip
$T$      =    temperature
$u, v, w$      =    velocity components
$\xi, \eta, \varsigma$      =    local curve-linear coordinates
$y_n$      =    local normal distance from cone surface
$\alpha$      =    streamwise wave number
$\omega$      =    angular frequency
$\mu$      =    viscosity
$\rho$      =    density
$\tau$      =    shear stress
Superscript *    =    dimensional quantity
Subscript $\infty$    =    freestream quantity

---

[1] Graduate Student Researcher, MAE Department, UCLA, and AIAA Student Member. jxlei@ucla.edu
[2] Professor, MAE Department, UCLA, and AIAA Associate Fellow. xiaolin@seas.ucla.edu

# I.    Introduction

The success of transition and related heating prediction relies on the good understanding of the relevant physical mechanisms leading to transition. In spite of considerable efforts in experimental, theoretical, and numerical studies, many critical physical mechanisms underlying hypersonic boundary-layer transition are still poorly understood. Engineering design of hypersonic vehicles has mainly been based on transition criteria obtained by empirical correlations of experimental data. The $e^n$ method, which predicts boundary layer transition based on normal-mode linear stability theory, is by far the most successful mechanism-based prediction method for transition prediction. Nevertheless, the $e^n$ method suffers from a major drawback that it does not consider the effects of receptivity of the boundary layer to various freestream disturbance conditions. In reality, the transition location is highly depended on  the level of forcing disturbances[1].

Because of the difficulties in conducting hypersonic experiments and the complexity of hypersonic flows, fundamental hypersonic studies will increasingly rely on the use of direct numerical simulations (DNS). In order for a DNS technique to perform reliable "numerical experiments", it is necessary to develop high-order accurate numerical algorithms suitable for highly accurate simulation of high-speed flows. Due to the enormous requirement on computer power and memory, DNS studies on boundary layer transition have been limited to idealized cases of boundary layer response to imposed forcing waves. So far, the complete process of laminar-turbulent transition from leading edge to the beginning of transition has not been computed by direct numerical simulation. Such a task has been commonly regarded as beyond the capability, in terms of computer times and memory, of currently available computers. On the other hand, if possible, such simulation can have significant impact on the state of the art in transition prediction because the effects of freestream disturbance level on transition location can be predicted by DNS. We believe that with our proposed simulation method and the availability of large scale parallel computation power, we can tackle the problem of DNS of hypersonic boundary layer transition.

Therefore, the purpose of this paper is to develop, demonstrate, and validate a robust and reliable DNS computational tool for the numerical simulation of the complete process of hypersonic boundary layer transition. Such simulation tool can be valuable in the prediction of surface heat transfer rates in transitional hypersonic boundary layers. The DNS can also calculate the heat transfer overshoot at transition. Our main idea is to use DNS to compute the complete transition process under realistic freestream noise and disturbances by dividing it into a three step process. In addition, we have been awarded the teragrid computer resources for the current project.

Since 1990s, significant progress has been made by several research groups in DNS studies of fundamental mechanisms leading to nonlinear breakdown and transition of supersonic and hypersonic boundary layers [2-4]. In DNS studies, the full 3-D nonlinear Navier-Stokes equations are computed to simulate the development and nonlinear interaction of the disturbances waves. A number of transition mechanisms have been identified and studied. In some cases, transition was simulated up to the beginning of turbulence. Detailed information on the formation and evolution of transitional flow structures, as well as average heating rates and skin friction, could be obtained by the simulation. It was found that the transition mechanisms for supersonic boundary layers include secondary instability of either sub-harmonic or fundamental resonances [5]. By using DNS, Thumm [6] and Fasel et al. [7] discovered a new breakdown mechanism for a boundary layer at Mach 1.6, which they termed oblique breakdown. This breakdown to turbulence is initiated by the nonlinear wave interaction of two oblique instability waves with equal but opposite wave angles. The mechanisms have also been confirmed by many researchers, including Chang and Malik [8]. For supersonic flows, it was shown that oblique breakdown leads to a more rapid transition than the secondary instability mechanisms. It also requires much lower threshold disturbance amplitudes for the nonlinear development [9]. For these reasons, oblique breakdown has been suggested to be of practical importance for supersonic transition in low-disturbance environments [10, 11].

Husmeier and Fasel [12] did DNS studies of secondary instability mechanisms of hypersonic boundary layers over cones with a circular cross section. The computational domain is a cut-out section of the whole flow field (*Fig.1*). Though hypersonic boundary layer is most unstable to second-mode two-dimensional waves, their investigations indicated that secondary instability mechanisms involving two-dimensional waves appear to be of lesser importance in the nonlinear stages of breakdown. Instead, second-mode oblique waves at small wave angles, which are almost as amplified as second-mode two-dimensional waves, were found to dominate the nonlinear behavior. It seems that further studies are necessary in order to confirm this conclusions because extensive

experimental results have pointed toward the dominant of 2-D second mode before transition in hypersonic boundary layers [13, 14].
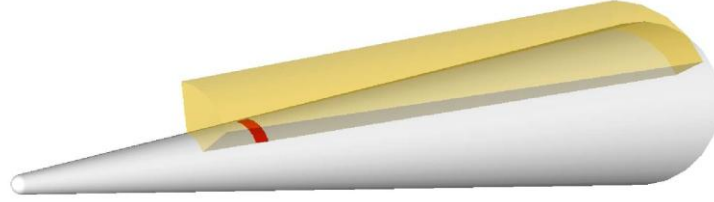


**Fig.1. Computational domain used in Husmeier and Fasel's DNS simulation [12].**

For hypersonic boundary layer transition, Pruett and his colleges did spatial DNS of hypersonic boundary layers of Mach 8 flow over a cone of eight-degree half angle [2, 3, 15]. The transitional state was triggered by a symmetric pair of oblique second-mode disturbances whose nonlinear interactions generate strong streamwise vorticity, which leads severe spanwise variations in the flow and eventual laminar breakdown. In their simulations, the PSE method was used to compute the weakly and moderately nonlinear initial stages of the transition process and, thereby, to derive a harmonically rich inflow condition for the DNS. The strongly nonlinear and laminar-breakdown stages of transition were subsequently computed by well-resolved DNS.
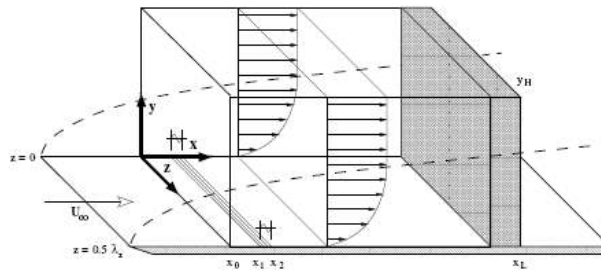


**Fig.2. A typical DNS simulation domain on a flat–plate boundary layer.**

However, most of the previous DNS research of compressible boundary layers has been mainly focused on supersonic flow of Mach less than 5 and on simplified flow over flat plates (*Fig.2*). In addition, the simulation was not related to practical flows because only theoretical or artificial forcing waves were used to study transition mechanisms. To date, with the exception of Rai and Moin [16], virtually all of the numerical experiments have simulated controlled rather than natural occurring instability processes. In a controlled experiment, instability waves of a particular wavelength (spatial) or frequency (temporal) are excited by imposed forcing. In contrast, in natural transition, the input is random, and the flow itself selects the preferred instability modes. A few of the cited simulations are hybrid in the sense that the primary instability wave is imposed, whereas secondary instability is triggered by low-level noise [17, 18].

The objective of the paper is to perform non-linear simulation with the inflow disturbance that is induced by the freestream waves. A linear receptivity database are built and used to construct the inflow disturbance spectrum that resembles the freestream profile of either flight environment or experiment. The simulation will be carried out to reach the non-linear and eventually the breakdown stage in transition. It is expected that the success of this DNS will help in understanding the effects of freestream disturbance levels to the location of the non-linear breakdown. Also, once the approach is proved successful, it will provide a reliable tool in predicting the transition in hypersonic boundary layer.

## II.    Numerical Method and Solution Strategy

### A.  Governing Equations

The governing equations are the unsteady compressible 3D Navier-Stokes equations. The advantage of solving the full Navier-Stokes equations is that it contains least amount of approximation such that, if implement correctly, it can resolve the flow field with very high accuracy. They can be written in the following conservative form:

$$\frac{\partial U^*}{\partial t^*} + \frac{\partial F_j^*}{\partial x_j^*} + \frac{\partial F_{vj}^*}{\partial x_j^*} = 0 \tag{1}$$

where $U^* = (\rho^*, \rho^* u_1^*, \rho^* u_2^*, \rho^* u_3^*, e^*)$, and superscript "*" represents dimensional variables. The $F^*$ s are invicid and viscous flux terms that can be expanded as

$$F^*_j = \begin{Bmatrix} \rho u_j \\ \rho u_{j1} u_j + p\delta_{1j} \\ \rho u_{j2} u_j + p\delta_{1j} \\ \rho u_{j3} u_j + p\delta_{1j} \\ (e+p)u_j \end{Bmatrix} \quad \text{and} \quad F^*_{vj} = \begin{Bmatrix} 0 \\ \tau_{1j} \\ \tau_{2j} \\ \tau_{3j} \\ \tau_{jk}u_k - q_j \end{Bmatrix} \tag{2}$$

The Cartesian coordinates are denoted by $(x_1^*, x_2^*, x_3^*)$ in tensor notation. In the current simulation of axisymmetric flow over blunt cones, $x^*$ is the coordinate along the centerline of the cone pointing toward the downstream direction. The origin of coordinate is co-located with the center of spherical nose.

### B.  Numerical Scheme

A High-order shock-fitting method developed by Zhong [19] is used to compute the flow field bounded by the bow shock and cone surface. The flow variables behind the shock are determined by Rakine-Hugoniot relations across the shock and the characteristic compatibility equations. Since the performance of the linear stability analysis is very sensitive to the base flow solution, the base flow must be very accurate in order to obtain the reliable results on the linear stability analysis.  The shock-fitting scheme had been tested and proven accurate and reliable by different test case.

### C.  Solution Strategy

We propose to tackle this problem by using our innovative approach of separating the linear receptivity simulation from the nonlinear breakdown simulation. In this way, we are able to make the computational cost manageable by breaking the whole simulation process into 3 major steps:

- **Step I: Mean Flow Simulation**. The high accuracy mean flow solution without any freestream disturbance is obtained using our high-order shock-fitting code. This is done with multiple zone procedure by cutting the whole computational zone along the cone surface into shorter subzones and marching the solution downstream as long as we needed.

- **Step II**: **Linear Receptivity Simulation.** In step two, a series of linear receptivity simulations are carried out with different types of freestream disturbances: fast acoustic wave, slow acoustic wave and entropy wave. They are imposed in the receptivity simulation to the mean flow solution in the freestream. In the receptivity simulation of each type of disturbance, multiple frequencies are imposed to better represent the freestream wave spectrum. The receptivity simulation will be carried all the way to the end of the linear growth region. This location can be estimated by LST analysis or by investigation of simulation result. The linear receptivity simulation is computationally much less expensive than the full scale 3D non-linear simulation due to the fact that the simulation is axis-symmetric in nature. So, a 2D simulation with significant less number of grid points is sufficient. Currently, the linear receptivity calculations for fast and slow acoustic wave have been completed.

- **Step III**: **Non-linear Breakdown Simulation**. After finishing the receptivity simulation, the entrance condition for the 3D non-linear simulation can be constructed based on the solutions obtained from the linear simulation. Since the Fourier decomposition in time can be applied to separate the solution in linear region for different frequencies, we can rescale the magnitude of solution for each specified frequency to match the freestream noise spectrum in a typical experiment. Therefore, the complete transition process due to different freestream noise profile can be simulated by using the receptivity results. So that, we just need to do the receptivity simulation once for different cases of different freestream spectra and different noise amplitudes. We can simply rescale the magnitude of each frequency to match the freestream value in the spectrum. As a result, for various freestream disturbance profiles, only step three is repeated to investigate the effects of freestream noise levels on the location of boundary layer transition.
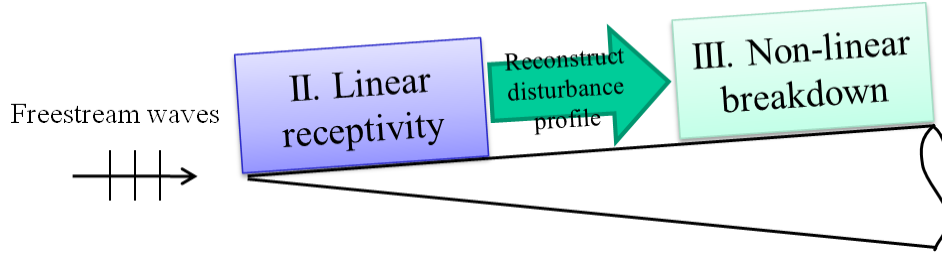


**Fig. 3. Schematic of proposed simulation procedures to non-linear breakdown**

## III.  Computation Setup

### A. Flow Conditions and Models

In this paper, we will mainly use Stetson's Mach 5.5 test case[20] for code testing purpose, even though the approach can be easily applied to other cases. The specific flow conditions are:

- $M_\infty = 5.468$
- $P_\infty^* = 7756.56\,Pa$, $T_\infty^* = 174.46K$
- Wall temperature: $T_w = 296K$
- $\gamma = 1.4$, $\mathrm{Pr} = 0.72$, $R^* = 286.94\,Nm/kgK$
- Freestream unit Reynolds number: $\mathrm{Re}_\infty^* = 18.95 \times 10^6\,m^{-1}$

- Blunt cone half angle: $\theta = 8^\circ$, the freestream flow has a zero angle of attack
- Parameters in Sutherland's viscosity law: $T_r^* = 288K$, $T_s^* = 110.33K$,

$$\mu_r^* = 0.17894 \times 10^{-4} kg / ms$$

We have already obtained the mean flow solutions for cones with three different nose radii in previous study. In this paper, we will carry out the non-linear breakdown simulation placing the focus on the case with nose radius of 0.156 inch.

## B. Boundary Conditions

The inflow boundary condition is obtained from the preceding linear receptivity simulations. Fourier decomposition is applied to separate disturbance waves into different frequencies. Therefore the inflow disturbance can be from freestream fast/slow acoustic wave, entropy waves and combination of all. In this paper, we only focus on using the disturbance profile from freestream fast acoustic waves for code testing purpose. A more realistic disturbance profile can be constructed to be consistent with those from typical experiments.

At the cone surface, non-slip boundary cone is enforced for the velocities. The cone surface temperature is fixed at 296 K, which is considered as a cool-wall boundary.

At the shock, the freestream waves are temporary turned off which is believed to have minimal impact to the simulation result.

At the exit, a sponge layer needs to be employed to damp out the numerical reflection. The detail formulation and implementation is explained later.

In the span-wise direction, for the 3D simulation, only a quarter of the cone is computed with the periodic condition imposed.

## C. Sponge Layer

For the non-linear portion of the unsteady simulation, a sponge layer needs to be added to the outflow to avoid spurious reflection and blowing up. In the sponge layer, an additional term is used to force the solution toward target values as shown in eq. (3). $U$ is the place holder for any conservative variable. $A(\xi)$ is a weight function smoothly increases from 0 to 1. The steady flow values are used as the reference values in the equation, so that the flow will be forced back to laminar state. Fig. 4 shows the test case which the sponge layer is added at the exit of computational domain. It clearly demonstrates that the sponge layer damps out the disturbance wave quickly with no numerical reflection.

$$\frac{dU}{dt}\bigg|_{adj} = \frac{dU}{dt} - \sigma A(\xi)\left[U - U_{ref}\right] \tag{3}$$

$$A(\xi) = \frac{1}{t_{ref}} e^{-\xi^4/10}(1 - \xi^{50})^4 \tag{4}$$

$$t_{ref} = \frac{u_\infty}{L_{buf}} \tag{5}$$

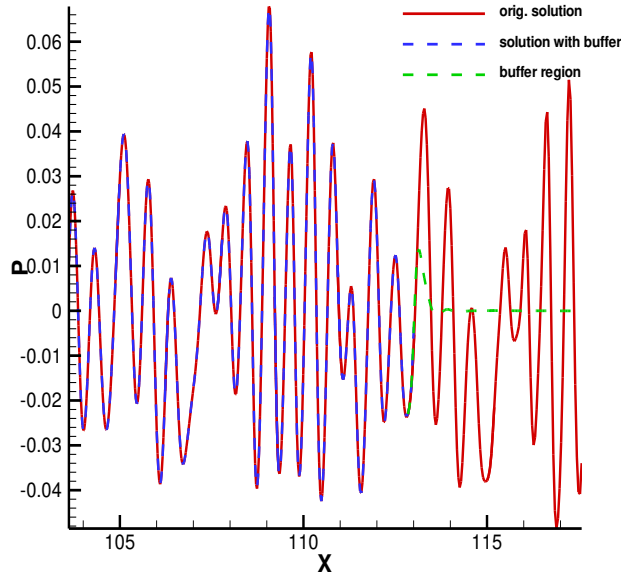$$\xi = \frac{x_L - x}{L_{buf}} \quad (1 \geq \xi \geq 0) \tag{6}$$

**Fig. 4. Comparison of solutions before and after the buffer is enforced.**

## IV.    Results

The mean flow and linear receptivity are presented in another paper by Zhong and Lei [21]. In that paper, the detail mean flow results for cones of three different nose radii are presented.  Also, the linear receptivity simulation results by the freestream fast acoustic waves are reported. In the current paper, the focus is placed on the development and the results of the non-linear simulation.

For code development purpose, 3 cases of non-linear simulations are carried out as summarized in Table 1. The test case 1 is a 2D simulation to check out the performance of the newly developed sponge layer. It also serves the purpose of understanding the non-linear interaction between different frequencies in such a simulation. The random white noise is added to the inflow disturbance just to enrich the spanwise wave number spectra for 3D simulation. Therefore, it is not necessary in the 2D case. However, the white noise is kept in the 2D simulation for code development reason. Test case 2 and 3 are true 3D simulation with grids in azimuth direction to capture the growths of spanwise wave numbers. For all the test cases, only disturbances from freestream fast acoustic waves are forced at the inlet of computation domain.

**Table 1. Test cases conducted on non-linear simulation**

| Test case | Disturbance level | Grid | Domain length |
|-----------|-------------------|------|---------------|
| 1 | Primary wave: 5%+ White noise: 0.05% | 3200×240×1 | 0.41 m ≤ X ≤ 0.8 m |
| 2 | Primary. wave: 5%+White noise: 0.05% | 3200×240×128 | 0.41 m ≤ X ≤ 0.8 m |
| 3 | Primary wave: 2%+ White noise: 0.05% | 6400×560×64 | 0.41 m ≤ X ≤ 1.1 m |

## A. 2D Non-linear Simulation

As a preliminary test, a 2D non-linear unsteady simulation is conducted with the inflow disturbance from the freestream fast acoustic wave. The overall freestream disturbances amplitude in the simulation is set to 5% of the freestream pressure values. In Fig. 6, computational grid mesh is showed with every 50th grid showed in streamwise direction and every 30th grid showed in the wall-normal direction. In streamwise direction, the gird is uniformly distributed, while the wall-normal gird is stretch toward the wall in order to well resolve the boundary layer. In this unsteady simulation, total 15 equally distributed disturbance waves are imposed with frequencies ranging from 52.55 kHz to 797.05 kHz. From a previous linear stability (LST) study of the current case [22], the axis-symmetric second-mode instability frequencies are identified as shown in Fig. 6. According to LST, the 12th and 13th frequencies should be the most dominant frequencies in the region of interest.
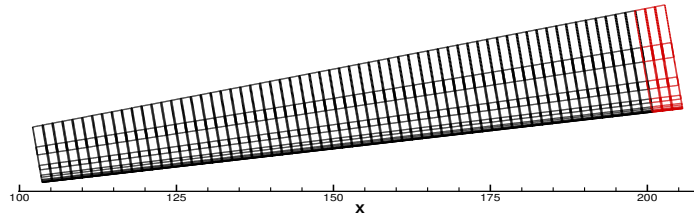


**Fig. 5. Grid of the 2D unsteady simulation with the sponge layer indicated in red.**
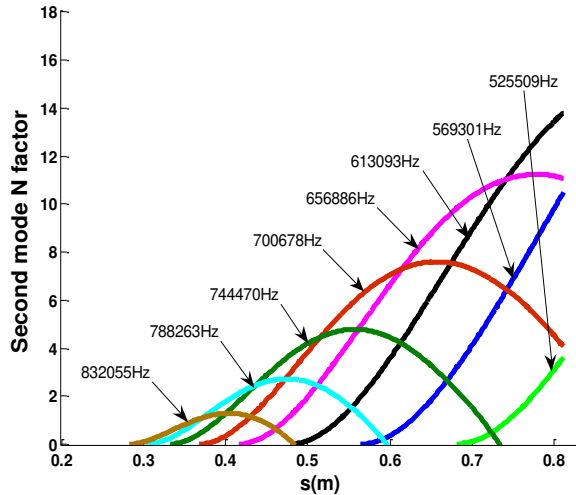


**Fig. 6. Linear Stability (LST) N factor for the Stetson's Mach 5.5 case with 0.156 inch nose[22].**

As shown in Fig. 7, even though the forcing waves' amplitudes are non-linear, the region is still under second-mode dominant. Both pressure along the surface and the *u* velocity above the surface show strongly growth of second-mode instability. From the pressure perturbation amplitude figure, the disturbance wave at 12th frequency (F12 = 630 kHz) reaches saturated level at x = 0.7 m while the LST calculation (Fig. 6) predicts a further growth at the same frequency. The u velocity perturbation amplitude figure reveals an interesting interaction between the mean flow distortion levels and the growth of second-mode instability in the non-linear region. The mean flow distortion level increases as the 13th frequency wave amplifies initially. As the 13th frequency wave decades, the mean-flow distortion levels drop quickly. However, it starts to increase again when the wave at lower frequency starts to grow. Also, due to the fact that the disturbance wave at the 12th frequency reaches saturation level, the growth of disturbance wave at lower frequencies are suppressed. F11 supposes to grow at further downstream location according to LST calculation, but it does not appear to grow at all in this non-linear case.
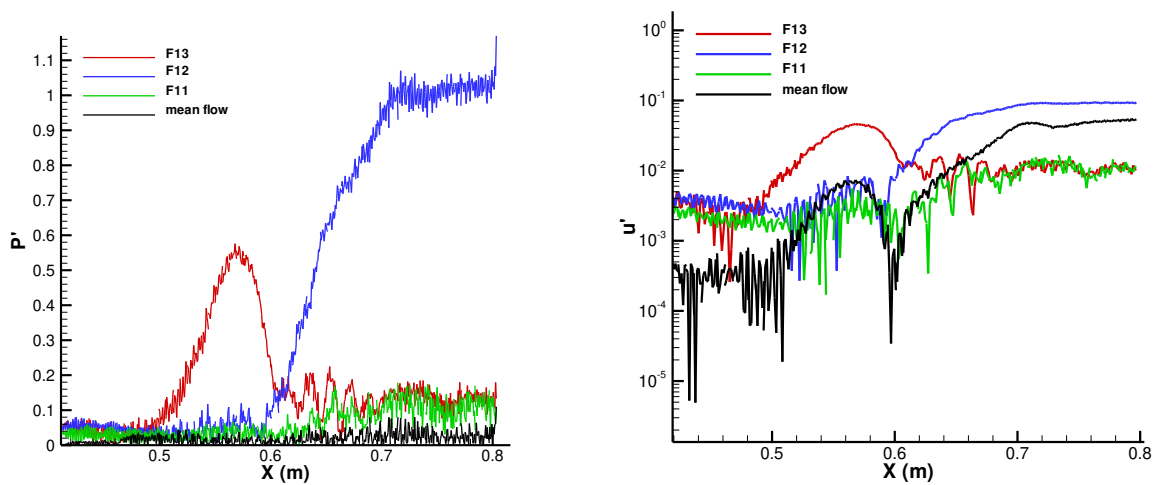
**Fig. 7. Pressure (L) and *U* velocity (R) disturbance amplitudes for selected wave frequencies.**

## B. 3D Non-linear Simulation

To simulate the non-linear breakdown during transition, the growths of spanwise wave modes play a crucial important role. Therefore, it is more realistic to conduct a 3D simulation instead of pure 2D simulation. In the 3D non-linear simulation, only one quarter of the cone are computed with periodic conditions enforced in the spanwise direction.
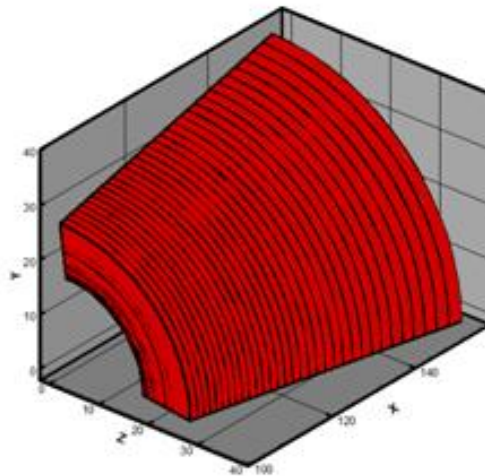


**Fig. 8.  Sample grid mesh of 3D simulation**

For the first 3D nonlinear simulation, the RMS amplitude of the primary forcing is set to 5% of the freestream pressure value. A 0.05% white noise is also added to it the primary waves to enrich the spanwise wave number spectra. The total length of computation domain is about 0.4 m long. In Fig. 9, the spanwise vorticity contours at the symmetric plane of the cone are presented. The development of the well known " rope-like" pattern is observed

starting from x = 0.6 m. Around x = 0.7 m, the "rope-like" pattern starts to roll up; and, at the same location, in the area close to the surface, the vorticity tends to break into small structure due to the high shearing right above the cone surface. However, for this particular test case, no three dimensional breakdown can be observed.
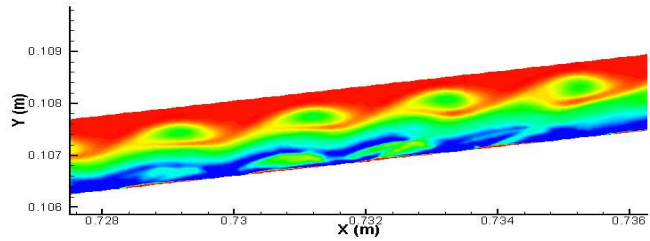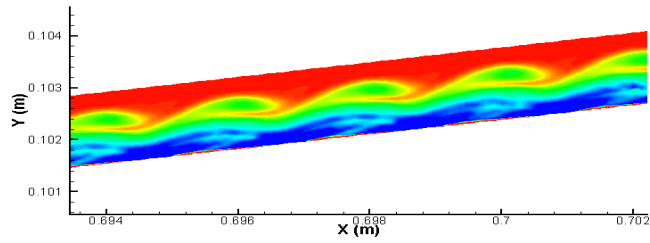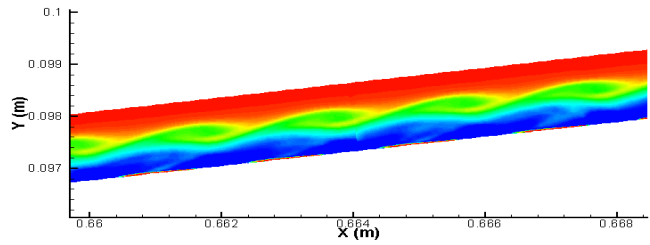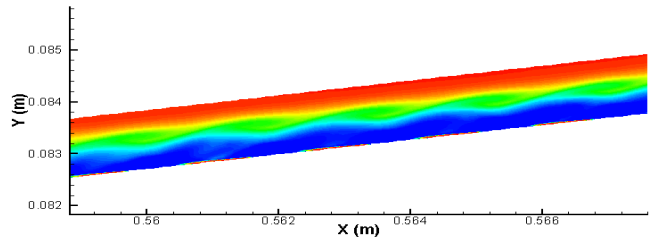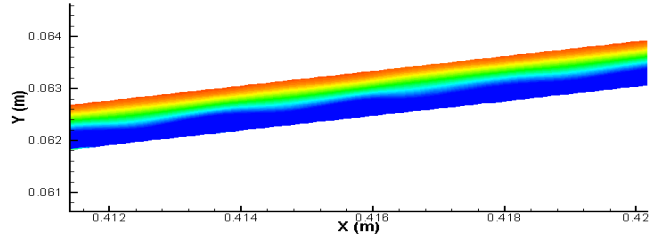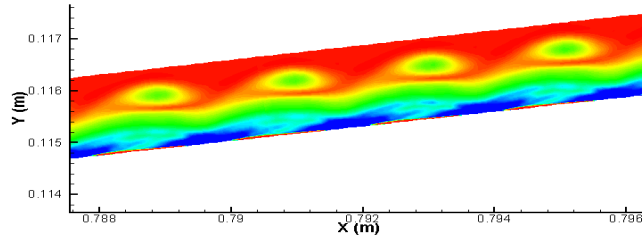
**Fig. 9. Spanwise vorticity contours on the symmetric plane of cone at different streamwise locations.**

In order to understand the key factor that triggers the nonlinear breakdown mechanism, the Fourier analysis is applied to study the behavior of each Fourier mode during the entire process. Fig. 10 shows the disturbance amplitudes of three primary waves which are the most unstable based on LST calculations. These primary waves have spanwise wave number k=0. Similar to the 2D case, the growths of disturbance waves are still second-mode dominant as shown in the pressure disturbance amplitude figure. The wave at the 12th frequency reaches saturation around x=0.7 m. As for the *u* velocity disturbance amplitude, no second-mode growths can be identified. The waves amplitudes are much higher than those of 2D simulation. All the selected waves start from initial amplitudes around $10^{-3}$ and grow 3 orders of magnitude when they move downstream.
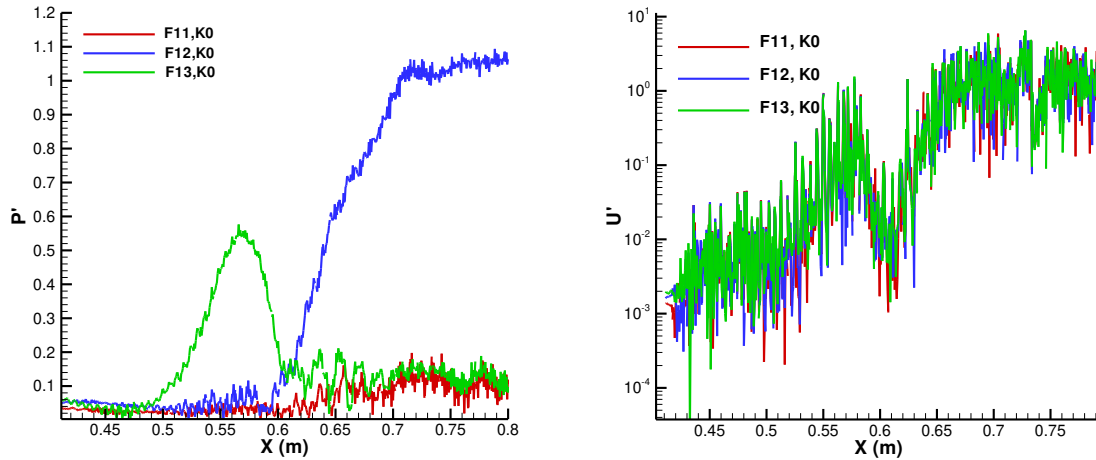


**Fig. 10. Perturbation amplitudes for selected wave frequencies with spanwise wave number k=0**

Since the higher spanwise wave number components play a crucial important role during the nonlinear breakdown process, they are also studied through Fourier analysis. For the current test case, a total of 128 grid points are assigned in the spanwise direction. Therefore, up to 64 spanwise wave modes can be resolved. Fig. 11 shows the *u* velocity disturbance amplitudes for different spanwise wave numbers. In these figures, F indicates the corresponding frequency and K represents the spanwise wave number. For the cone geometry, the spanwise wave number is discrete, while it can be continuous for the flat plane case. The growths for all wave numbers and different frequencies are very similar. Most of them start with initial amplitudes of $10^{-4}$ and grow to around $10^{-1}$, which is at least one order of magnitude lower than the amplitude of primary waves at the same location. It is believed that the breakdown occurs when the primary waves and higher spanwise wave number modes reach the same level in amplitude. In order to satisfy such a condition, we need to either increase the initial disturbance amplitudes of the higher wave number components or have a longer computational domain.
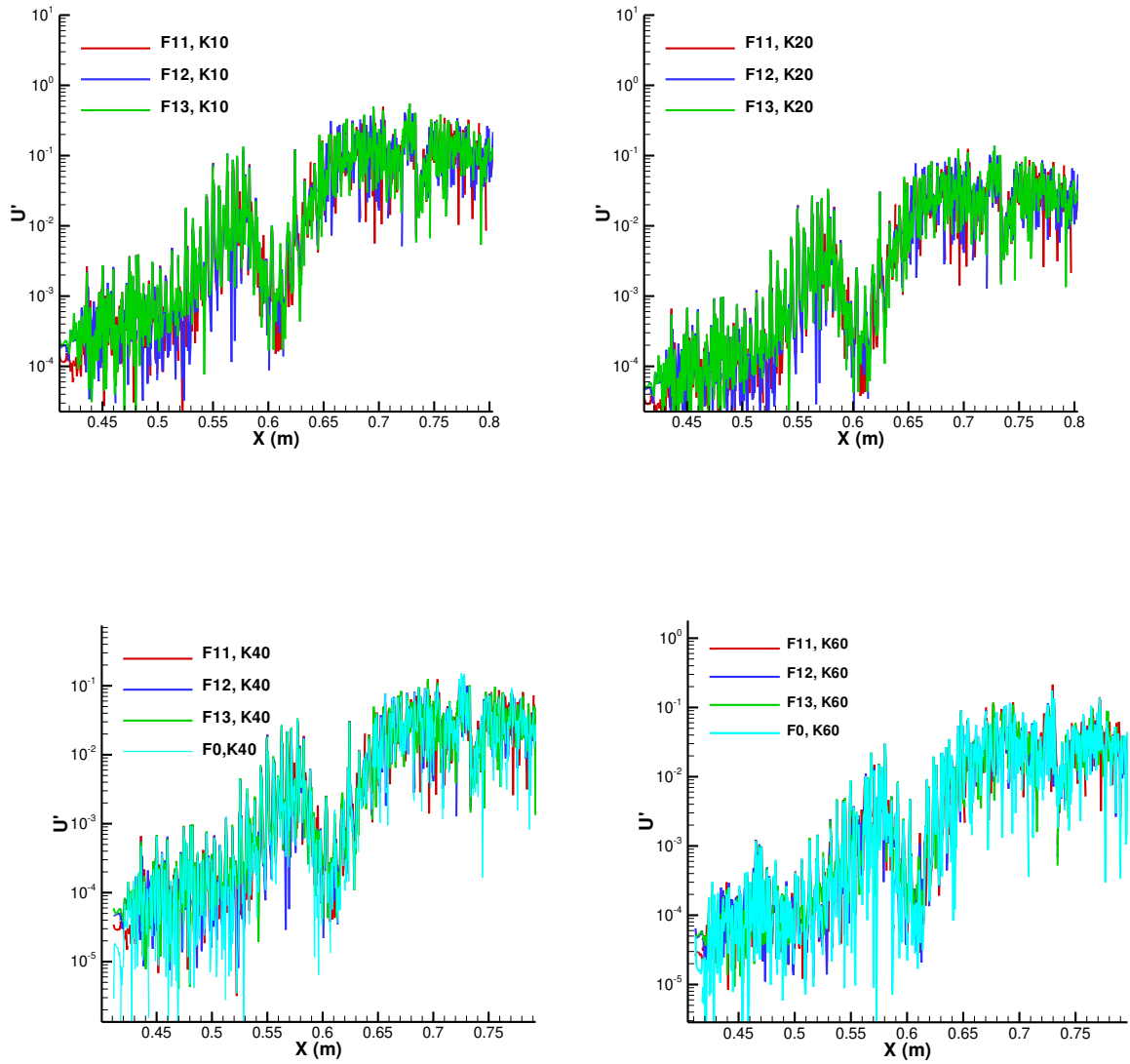
**Fig. 11.** *U* **velocity perturbation amplitudes in streamwise direction with different spanwise wave numbers.**

As discussed, the nonlinear breakdown has not been seen in the previous 3D simulation, a new case with a longer domain is set up. The new case has a total length about 0.7 m from x = 0.41 to 1.1 m. It is forced with slightly lower amplitude of 2% with the same level of white noise. Since this new case is still in transient stage, only the instantaneous vorticity contours are provided (Fig. 12) with emphasis on the later region. Also, the instantaneous perturbation profiles are shown in Fig. 13, which indicate that the perturbations are most amplified inside the boundary layer.
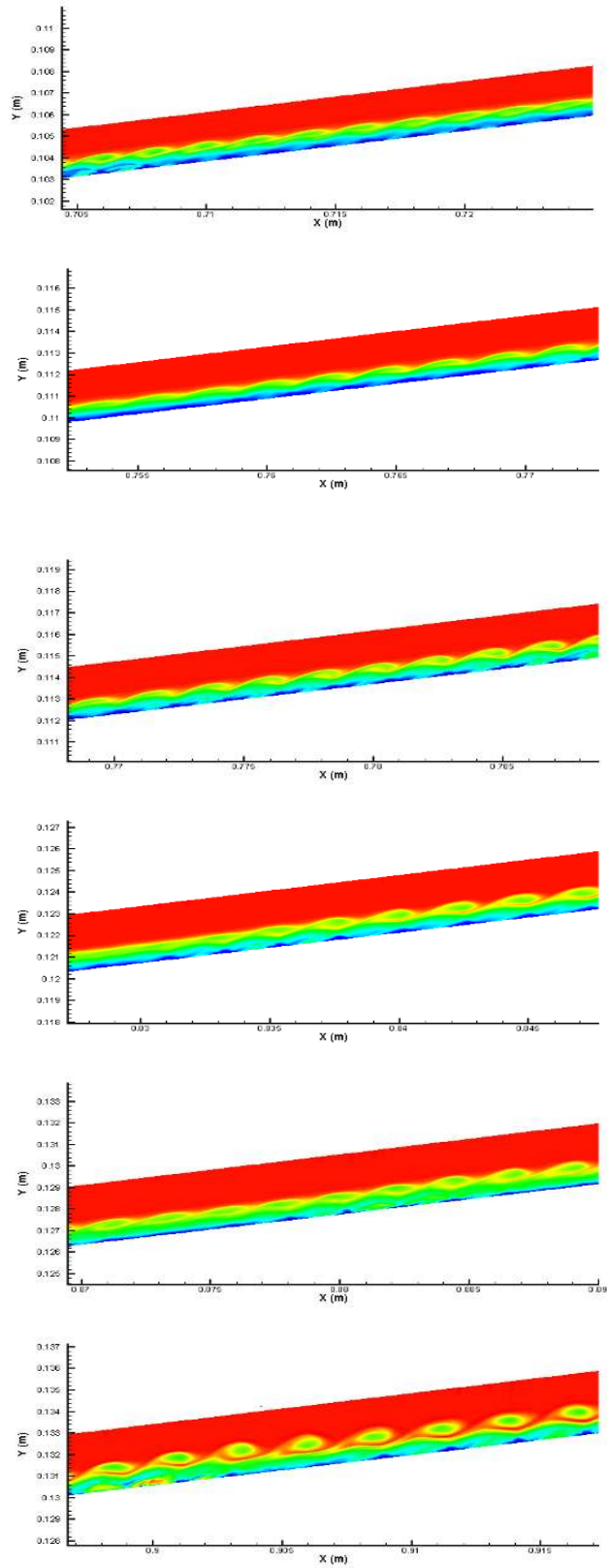
**Fig. 12. Spanwise vorticity contours on the symmetric plane of cone at different streamwise locations.**
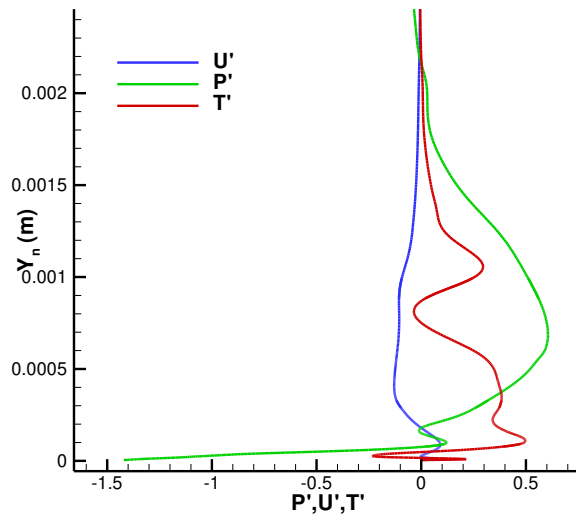
**Fig. 13. Instantaneous perturbation profiles at x = 0.91 m.**

# V.    Summary and Future Works

In this paper, we have demonstrated that, with our innovative approach, it is possible to conduct a 3D non-linear simulation and directly connect the freestream disturbance levels to the location of hypersonic boundary layer transition. However, the results presented here are still preliminary. We are in the effort to analyze and validate our current results. A new case with a longer computational domain is under computation which is more likely to reach the non-linear breakdown stage. Once this approach is proved feasible, we will construct a more practical freestream disturbance profile using our linear receptivity database and apply it to the future parametric study on freestream disturbance levels to hypersonic boundary layer transition.

## References

1.    Saric, W.S., Reed, H. L., and Kerschen, E. J., *Boundary-Layer Receptivity to Freestream Disturbances.* Annual Review of Fluid Mechanics, 2002. **34**: p. 291-319.
2.    Pruett, C.D., Zang, T. A., Chang, C. L., and Carpenter, M. H., *Spatial Direct Numerical Simulation of High-Speed Boundary-Layer Flows, Part I: Algorithmic Considerations and Validation.* Theoretical and Computational Fluid Dynamics, 1995. **7**: p. 49-76.
3.    Pruett, C.D.a.C., C. L., *Spatial direct numerical simulation of high-speed boundary-layer flows Part II: Transition on a cone in Mach 8 flow* Theoretical and Computational Fluid Dynamics, 1995. **7**: p. 397-424.
4.    Erlebacher, G., Hussaini, M. Y., *Numerical Experiments in Supersonic Boundary-Layer Stability.* Physics of Fluids A, 1990. **2**(1): p. 94-104.

5. Erlebacher, G.a.H., M. Y., *Stability and Transition in Supersonic Boundary Layers.* AIAA Paper 1987-1416, 1987: p. 1-12.

6. Thumm, A., Wolz, W., and Fasel, H. *Numerical simulation of spatially growing three-dimensional disturbance waves in compressible boundary layers*. in *Laminar-Turbulent Transition. IUTAM Symposium*. 1990. Toulouse, France,  1989 Springer-Verlag, Berlin.

7. Fasel, H., Thumm, A., and Bestek, H. *Direct numerical simulation of transition in supersonic boundary layers: oblique breakdown*. in *Fluids Engineering Conference, Transitional and Turbulent Compressible Flows*. 1993. Washington, DC, June 20–24, 1993: ASME, New York.

8. Chang, C.-L.a.M., M. R., *Oblique-mode breakdown and secondary instability in supersonic boundary layers.* Journal of Fluid Mechanics, 1994. **273**: p. 323-360.

9. Sandham, N.D., Adams, N. A., Kleiser, L., *Direct simulation of breakdown to turbulence following oblique instability waves in a supersonic boundary layer.* Applied Scientific Research, 1995. **54**: p. 223-234.

10. Mayer, C.S.J., von Terzi, D. A., and Fasel, H. F., *DNS of Complete Transition to Turbulence Via Oblique Breakdown at Mach 3.* AIAA paper 2008-4398, 2008: p. 1-21.

11. Laible, A., Mayer, C., and Fasel, H., *Numerical Investigation of Supersonic Transition for a Circular Cone at Mach 3.5.* AIAA paper 2008-4397 2008: p. 1-24.

12. Husmeier, F., Fasel, H. F., *Numerical Investigations of Hypersonic Boundary Layer Transition for Circular Cones.* AIAA paper 2007-3843, 2007: p. 1-17.

13. Stetson, K.F., Thompson, E. R., Donaldson, J. C., and Siler, L. G., *Laminar Boundary Layer Stability Experiments on a Cone at Mach 8, Part 1: Sharp Cone.* 1983. **AIAA Paper 83-1761**.

14. Stetson, K.F., Thompson, E. R., Donaldson, J. C., and Siler, L. G., *Laminar Boundary Layer Stability Experiments on a Cone at Mach 8, Part 2: Blunt Cone.* 1984. **AIAA paper 84-0006**.

15. Pruett, C.D.a.C., C. L., *Direct Numerical Simulation of Hypersonic Boundary-Layer Flow on a Flared Cone* Theoretical and Computational Fluid Dynamics, 1998. **11**: p. 49-67.

16. Rai, M.a.M., P., *Direct numerical simulation of transition and turbulence in a spatially evolving boundary layer.* AIAA Paper 91-1607, 1991: p. 890-912.

17. ADAMS, N.A., KLEISER, L., *Subharmonic transition to turbulence in a flat-plate boundary layer at Mach number 4.5.* Journal of Fluid Mechanics, 1996. **317**: p. 301-335.

18. Spalart, P.R., and Yang, K.-S., *Numerical study of ribbon-induced transition in Blasius flow.* Journal of Fluid Mechanics, 1987. **178**: p. 345-365.

19. Zhong, X., *High-Order Finite-Difference Schemes for Numerical Simulation of Hypersonic Boundary-Layer Transition.* Journal of Computational Physics, 1998. **144**: p. 662-709.

20. Stetson, K.F., Rushton, G. H., *Shock Tunnel Investigation of Boundary-Layer Transition at $M = 5.5$.* AIAA JOURNAL, 1967. **5(5)**: p. 899-906.

21. Zhong, X., Lei, J., *Numericla Simulation of Nose Bluntness Effects on Hypersonic Boundary Layer Receptivity tp Freestream Disturbances.* 2011. **AIAA paper 2011-3079**.

22. Lei, J., Zhong, X., *Linear Stability Analysis of Nose Bluntness Effects on Hypersonic Boundary Layer Transition.* 2010. **AIAA paper 2010-0898**.